



## Research paper

## 3,3'-OH curcumin causes apoptosis in HepG2 cells through ROS-mediated pathway

Guo-Yun Liu, Yong-Zheng Sun, Na Zhou, Xiu-Mei Du, Jie Yang<sup>\*</sup>, Shang-Jing Guo<sup>\*\*</sup>

School of Pharmacy, Liaocheng University, 1 Hunan Street, Liaocheng, Shandong 252000, China

## ARTICLE INFO

## Article history:

Received 24 October 2015

Received in revised form

4 February 2016

Accepted 5 February 2016

Available online 9 February 2016

## Keywords:

Curcumin

Hydroxyl group

Reactive oxygen species

Apoptosis

## ABSTRACT

In this paper, we synthesized a series of curcumin analogs and evaluated their cytotoxicity against HepG2 cells. The results exhibited that the hydroxyl group at 3,3'-position play an essential role in enhancing their anti-proliferation activity. More importantly, 3,3'-hydroxy curcumin (**1b**) caused apoptosis in HepG2 cells with the ROS generation, which may be mainly composed of hydroxyl radicals (HO<sup>•</sup>) and H<sub>2</sub>O<sub>2</sub>. The more cytotoxic activity and ROS-generating ability of **1b** may be due to the more stable in (RPMI)-1640 medium and more massive uptake than curcumin. Then the generation of ROS can disrupt the intracellular redox balance, induce lipid peroxidation, cause the collapse of the mitochondrial membrane potential and ultimately lead to apoptosis. The results not only suggest that 3,3'-hydroxy curcumin (**1b**) may cause HepG2 cells apoptosis through ROS-mediated pathway, but also offer an important information for design of curcumin analog.

© 2016 Elsevier Masson SAS. All rights reserved.

## 1. Introduction

Cancer chemoprevention uses agents that suppress the promotion and/or progression of premalignant cells has become an important approach to control cancer [1]. However, there are alarming obstacles that limit its chronic application due to long-term toxicity and the possibility of developing chemoresistance, and consequently search for an efficacy and safety strategy is ongoing. Excitingly, chemopreventive agents that enhance reactive oxygen species (ROS) reaching a toxic threshold can encourage apoptosis in cancer cells with minimal toxicity to normal counterparts [2,3]. A mild increase in the level of ROS may promote cell proliferation, whereas a severe increase of ROS in cancer cells could trigger cell death [1,4–9]. As their name suggests, ROS are oxygen-containing chemical reactive molecules including free radicals such as superoxide (O<sub>2</sub><sup>•-</sup>) and hydroxyl radicals (HO<sup>•</sup>), and non-radical molecules such hydrogen peroxide (H<sub>2</sub>O<sub>2</sub>) [5,10]. ROS are mainly produced in mitochondria electron transport chain and endoplasmic reticulum.

Curcumin, a nature cancer chemopreventive agent, can influence multiple signaling molecules such as protein reductase, cell

survival protein, inflammatory molecules and so on owing to its molecular structure and functionality [11–13]. Chemically, curcumin contains electrophilic Michael acceptor pharmacophore, two hydroxyl groups, two methoxy groups and an active methylene Michael donor unit [14]. Although curcumin has been shown to influence multiple signaling molecules, its instability and relatively low bioavailability have been highlighted as major problems [15,16]. In the last few decades, massive efforts have been made to search for new curcumin analogs without these drawbacks and with efficacy equal to or better than that of curcumin. Several independent groups revealed that some mono-carbonyl curcumin analogs exhibited much greater anticancer, antiangiogenesis activity [17–22] and antibacterium [23]. Our group's work was exploiting ROS-promoting signaling for designing curcumin-inspired anticancer agents and found that they can target TrxR and convert this antioxidant enzyme into a ROS promoter [24].

However, the structure-activity relationships (SAR) underlying cytotoxicity effects on cancer cells associated with curcumin analogs that contain electron withdrawing/donating groups is obscure and poorly understood. Whether these analogs inspired by curcumin caused generation of ROS to trigger cancer cell apoptosis? Spurred by the above challenges, we designed and synthesized a series of curcumin analogs with electron withdrawing/donating groups (–CF<sub>3</sub>, –OH, –OCH<sub>3</sub>) attaching to 2-, 3- or 4- position on the aromatic ring (Fig. 1). Thus we focus on the SAR underlying cytotoxicity and explore the apoptotic mechanism associated with

\* Corresponding author.

\*\* Corresponding author.

E-mail address: [yangjie1110@163.com](mailto:yangjie1110@163.com) (J. Yang).

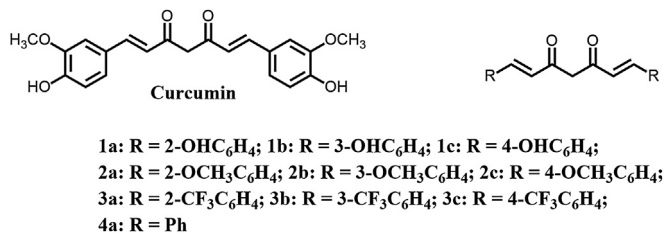


Fig. 1. Molecular structures of curcumin and its analogs.

curcumin analogs.

## 2. Results and discussion

### 2.1. Cytotoxicity and SAR

We started our studies with a comparison of the cytotoxicity of curcumin with its analogs on Human liver hepatocellular carcinoma cells (HepG2) by means of a MTT-based viability assay. The IC<sub>50</sub> values listed in Table 1 allowed us to identify the following SAR. (1) The curcumin analogs with the *meta*-substituent (–OH, –OCH<sub>3</sub>) on the aromatic ring(s) were more active than their corresponding *ortho*- and *para*-substituted compounds. (2) All of the curcumin analogs with the hydroxyl group exhibited the increased cytotoxicity compared to other bis-substituted (–OCH<sub>3</sub> or –CF<sub>3</sub>) compounds. (3) The cell-killing effects of **1b** with *meta*-hydroxyl on the aromatic ring(s) was stronger than that of leading curcumin. Especially, **1b** surfaced as an important lead compound displaying almost 3.5-fold cytotoxicity relative to curcumin. This results may be related to that **1b** in RPMI 1640 supplemented with 10% (v/v) heat-inactivated fetal calf serum was more stable than curcumin (Fig. S1 in the supporting information).

### 2.2. Induction of apoptosis via ROS-dependent pathway

To investigate the cytotoxic mechanism of curcumin analogs (**1b**), we also determined their effects on cell apoptosis by using flow cytometry. It was found that **1b** was a potent inducer of apoptosis and showed obvious dose-dependent. Specially, after treating HepG2 cells with 50 μM **1b** caused 80.2% late apoptosis (Fig. 2). Interestingly, pretreatment of glutathione (GSH) or N-acetylcysteine (NAC), the ROS scavenger, almost completely reversed the apoptosis induced by **1b**, preliminarily indicating the involvement of ROS (Fig. 2).

### 2.3. Intracellular ROS accumulation

Based on the above observation, we further employed the oxidation-sensitive probe, 2',7'-dichlorofluorescein diacetate (DCFH-DA) to measure the intracellular ROS levels by flow cytometry. As shown in Fig. 3A, **1b** caused a substantial increase in the

ROS levels in a dose- and time-dependent fashion. Especially, **1b** induced significantly higher ROS accumulation than curcumin (Fig. 3A). More importantly, the maximum ROS accumulation with a 5-fold increase relative to the control, was observed after treatment with 50 μM **1b** for 6 h. The stable and high ROS-generating ability should be responsible for the better cytotoxicity of **1b**. The results also may indicated a tight link among the ROS-generating ability, cytotoxicity and apoptosis-inducing activity.

ROS are mainly composed of superoxide (O<sub>2</sub><sup>•-</sup>), hydroxyl radicals (HO•) and hydrogen peroxide (H<sub>2</sub>O<sub>2</sub>). However, DCFH-DA is a widely used fluorescent probe to measure the intracellular ROS levels. To further clarified the role of ROS and specified their type, we used the catalase (CAT), the H<sub>2</sub>O<sub>2</sub>-scavenging enzyme and dihydroethidium (DHE), a relatively specific probe for O<sub>2</sub><sup>•-</sup> for next step. As shown in Fig. 3B, the increased DCF fluorescence in the cells treated with 50 μM **1b** was significantly reversed by CAT, clearly indicating that the increased ROS are partly composed of H<sub>2</sub>O<sub>2</sub>. However, using DHE, we found that treatment of cells with 50 μM **1b** had no effect on the DHE fluorescence (Fig. 3C), hinting that O<sub>2</sub><sup>•-</sup> was not contributed to the increased ROS levels induced by **1b**. These results also indicated that the increased ROS are mainly composed of hydroxyl radicals (HO•).

### 2.4. Cell uptake

To further explain the cytotoxicity activity, ROS-generating ability and apoptosis-inducing activity of **1b** was stronger than that of leading curcumin, we also compared the cellular uptake of **1b** and curcumin in HepG2 cells. As shown in Fig. 4, **1b** exhibited the faster and more massive cell uptake than curcumin, which was well absorbed to reach a peak value after 1 h of incubation, but it was rapidly and even completely metabolism for 6 h. This results was in line with the ROS-generating ability of curcumin and **1b**. Take together, the faster and higher uptake of **1b** may partly explain why it has better cytotoxic activity than curcumin.

### 2.5. Falling apart of intracellular redox buffering system

Next, we tested if the ROS generation induced by **1b** could cause imbalance of cellular redox homeostasis. Because glutathione (GSH), the most abundant low-molecular-weight thiol in cells, is involved in maintaining intracellular redox status, the ratio of GSH and its disulfide GSSG can be used to estimate cell redox status [25]. We found that the ratios of GSH/GSSG were sharply decreased in a dose-dependent fashion after treatment with **1b** at the indicated concentrations. Especially, the ratio of GSH/GSSG with a 2-fold decrease relative to the control, was observed after treatment with 50 μM **1b** for 6 h (Fig. 5). More interestingly, the time points (3 h) for generating ROS and changing cell redox status by **1b** are almost the same. The results also indicated that there was a relationship between a burst in ROS and collapse of the redox buffering system.

### 2.6. The formation of malondialdehyde

The major components of plasma membrane lipids are the most vulnerable molecules to reactive oxygen species attacking and resulting in lipid peroxidation. Lipid peroxidation was increased as measured the amount of MDA, the biomarker of lipid oxidation. As shown in Fig. 6, **1b** caused a substantial increase in the formation of malondialdehyde in a dose-dependent fashion and the amount of MDA with a 1-fold increase relative to the control, was observed after treatment with 50 μM **1b** for 18 h. These results suggest that cell lipid peroxidation was induced by **1b** via the intracellular ROS accumulation.

Table 1  
Cytotoxicity of curcumin and its analogs against HepG2 cells.

Comps.	IC <sub>50</sub> (μM) <sup>a</sup>	Comps.	IC <sub>50</sub> (μM)	Comps.	IC <sub>50</sub> (μM)
<b>1a</b>	50.0 ± 2.7	<b>2a</b>	125.2 ± 7.8	<b>3a</b>	>200
<b>1b</b>	15.1 ± 2.2	<b>2b</b>	83.4 ± 8.0	<b>3b</b>	>200
<b>1c</b>	75.5 ± 4.2	<b>2c</b>	>200	<b>3c</b>	>200
<b>curcumin</b>	52.3 ± 1.1	<b>4a</b>	>200		

<sup>a</sup> The IC<sub>50</sub> value is the concentration of a compound tested to cause 50% inhibition of cell viability after 48 h of treatment, and is expressed as the mean ± SD for three determinations.

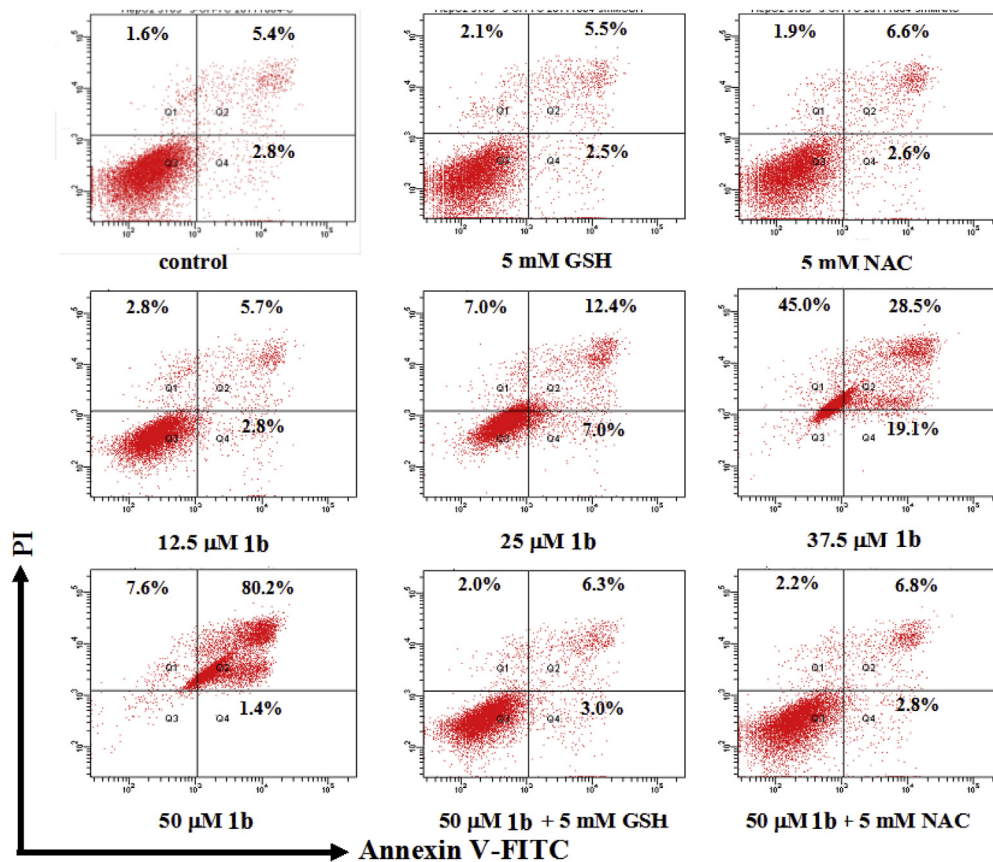


**Fig. 2.** Flow cytometric analysis for apoptosis induction of HepG2 cells after 24 h treatment with **1b** at the indicated concentrations in the absence or presence of 1 h pretreatment with GSH or NAC. Percentage of cells in early and late apoptosis and necrosis is indicated in each quadrant. Each experiment was performed in triplicate.

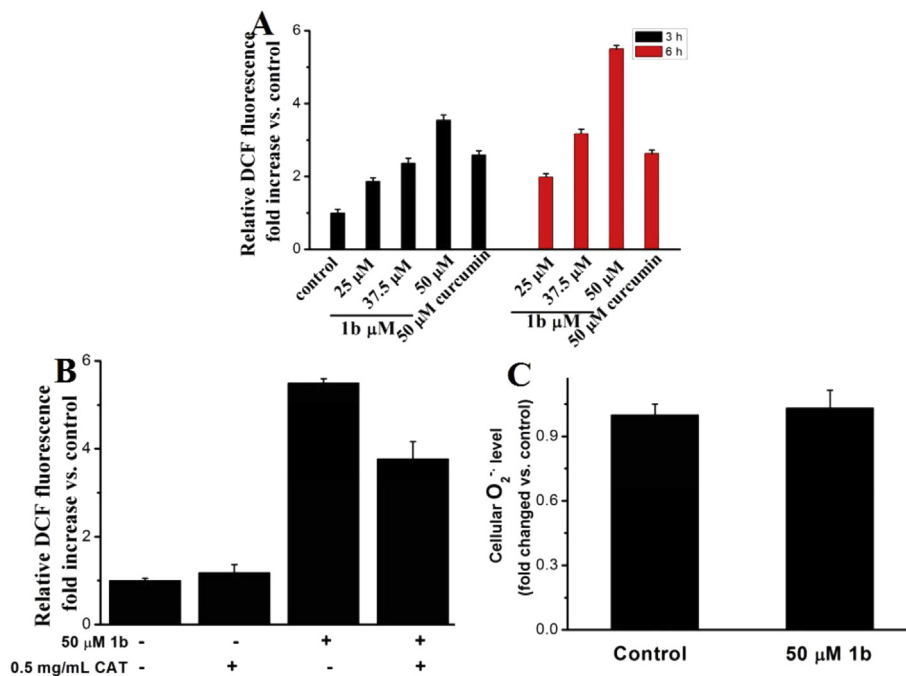


**Fig. 3.** (A) ROS generation induced by curcumin and its active analogs (**1b**) at the indicated concentrations and incubation time in HepG2 cells. (B) Effect of CAT on the increased ROS levels induced by **1b**. Cells were treated with 50 μM **1b** for 6 h in the absence or presence of 1 h pretreatment with CAT, and subjected to the DCFH-DA staining assay. (C) Alteration of the O<sub>2</sub><sup>-</sup> levels in the cells treated with **1b**. Cells were incubated with 50 μM **1b** for 6 h and stained with 3 μM DHE at 37 °C in the dark for 30 min, and analyzed by flow cytometry. Each experiment was performed in triplicate.

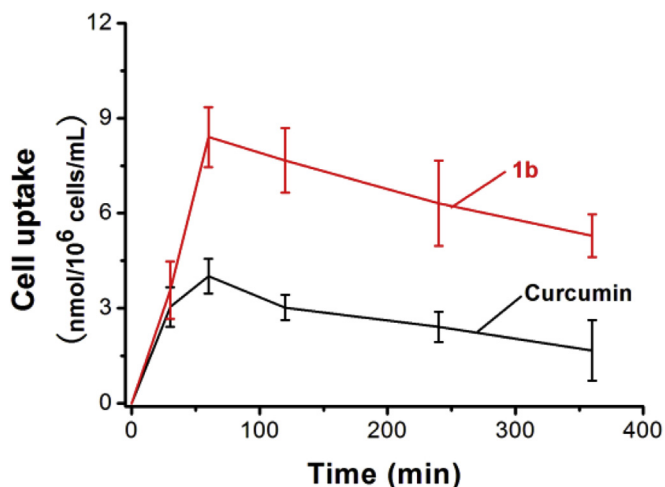


Fig. 4. Cellular uptake of curcumin and **1b** (50  $\mu\text{M}$ ) estimated by absorbance measurement of methanol-extracted cell lysates as a function of the incubation period.

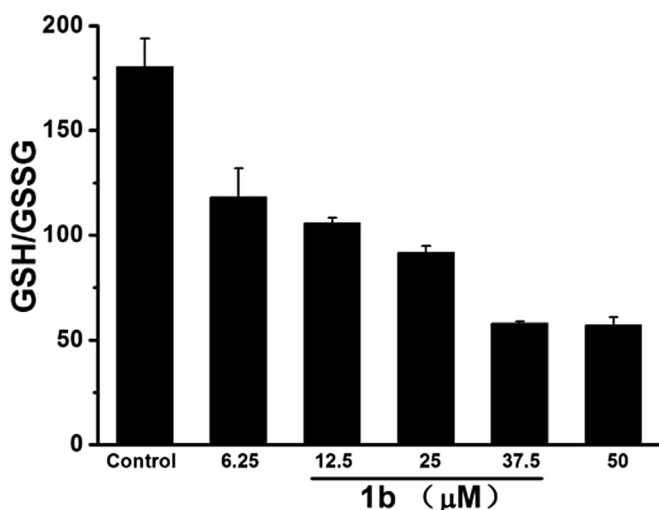


Fig. 5. Imbalance of redox homeostasis induced by **1b** in A549 cells. The GSH/GSSG ratios in cells after treatment with **1b** at the indicated concentrations for 6 h. Each experiment was performed in triplicate.

### 2.7. The collapse of mitochondrial membrane potential (MMP)

In order to determine the involvement of mitochondrial in **1b** mediated apoptosis in HepG2 cells, we monitored the changes on mitochondrial membrane potential with Rhodamine 123 by flow cytometry. As shown in Fig. 7, we found that **1b** was more active than the leading curcumin at the indicated concentrations in the collapse of mitochondrial membrane potential. It is a remarkable fact that **1b** showed perfectly time- and dose-dependent relationships. These results indicated that treatment of **1b** to HepG2 cells triggers the collapse of MMP.

### 2.8. The effects of GSH and NAC on the cytotoxicity, intracellular ROS accumulation and the collapse of mitochondrial membrane potential (MMP) induced by **1b**

In the above results, pretreatment of glutathione (GSH) or N-acetylcysteine (NAC), almost completely reversed the apoptosis induced by **1b**, preliminarily indicating the involvement of ROS (Fig. 2). To further elucidate whether ROS generation is directly

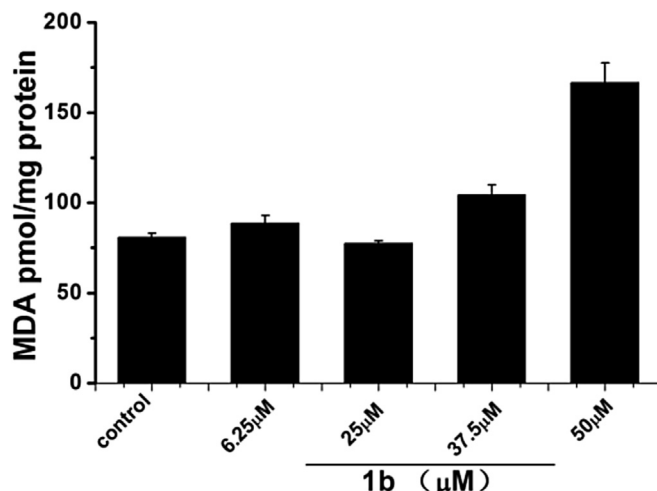


Fig. 6. MDA concentrations of HepG2 cells was determined after exposure to **1b** at the indicated concentrations for 18 h. Values are expressed as MDA equivalents (pmol)/mg protein. Each experiment was performed in triplicate.

associated with **1b**-elicited cytotoxicity and the collapse of mitochondrial membrane potential in HepG2 cells, cells were pretreated with ROS scavenger glutathione (5 mM GSH) or N-acetylcysteine (5 mM NAC) for 1 h, and then exposed to **1b** at the indicated concentrations. As expected, both GSH and NAC substantially reduced the ROS generation induced by 50  $\mu\text{M}$  **1b** in HepG2 cells (Fig. 8B). Furthermore, both GSH and NAC significantly blocked the cytotoxicity (Fig. 8A) and the collapse of mitochondrial membrane potential (Fig. 8C) induced by 50  $\mu\text{M}$  **1b** at the indicated time. These results went further to demonstrate that the cytotoxicity, apoptosis and the collapse of mitochondrial membrane potential were closely related with the ROS generation promoted by **1b**.

## 3. Conclusions

In conclusion, we synthesized a panel of curcumin analogs and investigated their biological mechanisms in inducing apoptosis of HepG2 cells. Compound **1b** surfaced as an important lead compound displaying the most potent cytotoxicity. Mechanistic investigation reveals that the compound could effectively promote the ROS generation, which may be mainly composed of hydroxyl radicals ( $\text{HO}\cdot$ ). The more cytotoxic activity and ROS-generating ability of **1b** may be due to the more stable in (RPMI)-1640 medium, more hydrophobicity and more massive uptake than curcumin. The ROS generation is associated with falling apart in the redox buffering system, and subsequently induces lipid peroxidation and collapse of mitochondrial membrane potential, ultimately leading to cell apoptosis (Scheme 1). This work not only suggest that 3,3'-hydroxy curcumin (**1b**) may cause HepG2 cells apoptosis through ROS-mediated pathway, but also offer an important information for design of curcumin analog.

## 4. Experimental

### 4.1. Reagents

Roswell Park Memorial Institute (RPMI)-1640 was from GIBCO. 2',7'-dichlorofluorescein diacetate, rhodamine 123, 3-(4,5-dimethylthiazol-2-yl)-2,5-diphenyltetrazolium bromide (MTT), Glutathione reductase (GR), the reduced (GSH) and oxidized (GSSG) glutathione, N-acetylcysteine (NAC), 2-vinylpyridine (97%) and thiobarbituric acid were obtained from Sigma. All other chemicals

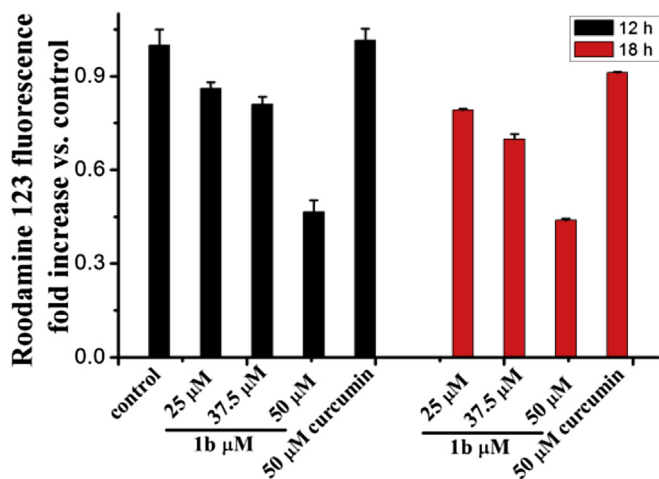


Fig. 7. Loss of mitochondrial membrane potential in HepG2 cells induced by **1b** at the indicated concentrations and time.

tributylborate (2 equiv) were added, and the mixture was stirred for 30 min *n*-Butylamine (1 equiv) dissolved in 10 mL of EtOAc was added dropwise over 20 min. Stirring was continued for 4 h at 40 °C. The mixture was then hydrolyzed by adding 10 mL of 1 N HCl and heating at 60 °C for 1 h. The organic layer was separated, and the aqueous layer extracted three times with EtOAc. The combined organic layers were washed with H<sub>2</sub>O, then dried over Na<sub>2</sub>SO<sub>4</sub>, and the solvent was removed in vacuo. The crude products were purified by silica gel column chromatography eluting with petroleum ether-EtOAc. The structures of curcumin analogs were confirmed by <sup>1</sup>H and <sup>13</sup>C NMR spectroscopy, HRMS (ESI), MS (The medium for HP-5988A GC-MS (EI) is MeOH.) and HPLC (see the [Supplemental Information](#)).

### 4.3. Spectroscopy data of compound **1a–4a**

#### 4.3.1. 1,7-Bis(2-hydroxyphenyl)-heptane-3,5-dione (**1a**)

Yield: 48%, yellow powder; R<sub>f</sub> = 0.35 (petroleum ether/EtOAc (2:1)); mp 171–172 °C; <sup>1</sup>H NMR 400 MHz (DMSO-*d*<sub>6</sub>), δ 10.2 (s, 2H),

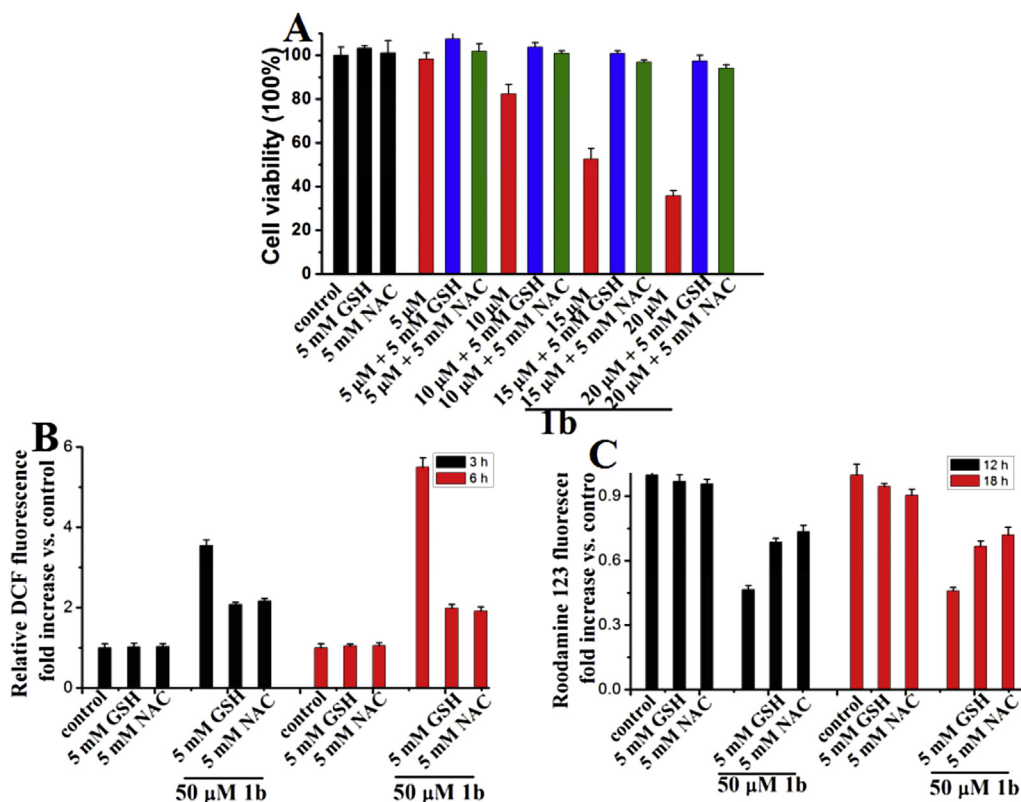


Fig. 8. (A) Effects of GSH (5 mM) and NAC (5 mM) on the cytotoxicity induced by **1b** at the indicated concentrations in HepG2 cells. (B) Effects of GSH (5 mM) and NAC (5 mM) on the ROS generation induced by 50 μM **1b** at the indicated time in HepG2 cells. (C) Effects of GSH (5 mM) and NAC (5 mM) on the collapse of mitochondrial membrane potential induced by 50 μM **1b** at the indicated time in HepG2 cells. Each experiment was performed in triplicate.

were of the highest quality available.

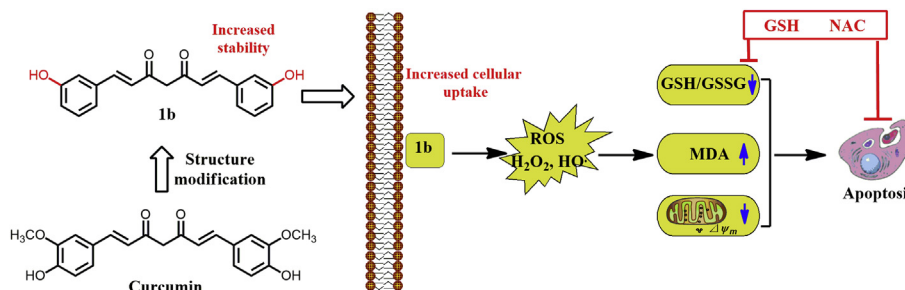
### 4.2. General procedure for the synthesis of curcumin analogs (**1a–4a**)

The curcumin analogs were synthesized according to the published procedure [26]. In general, 2,4-pentanedione (1 equiv) and boric anhydride (0.7 equiv) dissolved in 10 mL of EtOAc were stirred for 30 min at 40 °C. The appropriate benzaldehyde (2 equiv) and

7.86 (d, *J* = 16.0 Hz, 2H), 7.62 (d, *J* = 8.4 Hz, 2H), 7.22 (t, *J* = 8.0 Hz, 2H), 6.84–6.94 (m, 6H), 6.11 (s, 1H); <sup>13</sup>C NMR 100 MHz (DMSO-*d*<sub>6</sub>), δ 183.5, 156.8, 135.7, 131.5, 128.4, 123.5, 121.4, 119.5, 116.2, 101.5; MS (EI) *m/z* 308 [M]<sup>+</sup>.

#### 4.3.2. 1,7-Bis(3-hydroxyphenyl)-heptane-3,5-dione (**1b**)

Yield: 42%, yellow powder; R<sub>f</sub> = 0.32 (petroleum ether/EtOAc (2:1)); mp 198–200 °C; <sup>1</sup>H NMR 400 MHz (Acetone-*d*<sub>6</sub>), δ 8.56 (s, 2H), 7.60 (d, *J* = 15.6 Hz, 2H), 7.25 (t, *J* = 8.0 Hz, 2H), 7.15–7.19 (m,



**Scheme 1.** 3,3'-OH curcumin causes apoptosis in HepG2 cells through ROS-Mediated pathway.

4H), 6.90 (dd,  $J = 8.0, 1.6$  Hz, 2H), 6.79 (d,  $J = 8.0$  Hz, 2H), 6.12 (s, 1H);  $^{13}\text{C}$  NMR 100 MHz (Acetone- $d_6$ ),  $\delta$  184.6, 158.8, 141.4, 137.5, 131.0, 125.2, 120.7, 118.3, 115.5, 102.5; MS (EI)  $m/z$  308  $[\text{M}]^+$ .

#### 4.3.3. 1,7-Bis(4-hydroxyphenyl)-heptane-3,5-dione (**1c**) [26]

Yield: 51%;  $^1\text{H}$  NMR 300 MHz (Acetone- $d_6$ ),  $\delta$  7.58 (d,  $J = 15.9$  Hz, 2H), 7.55 (d,  $J = 8.7$  Hz, 4H), 6.89 (d,  $J = 8.7$  Hz, 4H), 6.64 (d,  $J = 15.9$  Hz, 2H), 5.98 (s, 1H);  $^{13}\text{C}$  NMR 75 MHz (DMSO- $d_6$ ),  $\delta$  184.6, 160.6, 141.1, 131.0, 127.7, 122.1, 116.9, 101.8; MS (EI)  $m/z$  308  $[\text{M}]^+$ .

#### 4.3.4. 1,7-Bis(2-methoxyphenyl)-heptane-3,5-dione (**2a**)

Yield: 52%, yellow powder;  $R_f = 0.35$  (petroleum ether/EtOAc (4:1)); mp 118–120 °C;  $^1\text{H}$  NMR 400 MHz ( $\text{CD}_3\text{Cl}$ ),  $\delta$  7.97 (d,  $J = 16.0$  Hz, 2H), 7.55 (d,  $J = 8.4$  Hz, 2H), 7.32 (t,  $J = 8.4$  Hz, 2H), 6.95 (t,  $J = 7.6$  Hz, 2H), 6.91 (d,  $J = 8.0$  Hz, 2H), 6.70 (d,  $J = 16.0$  Hz, 2H), 5.88 (s, 1H), 3.90 (s, 6H);  $^{13}\text{C}$  NMR 100 MHz ( $\text{CD}_3\text{Cl}$ ),  $\delta$  183.8, 158.3, 135.7, 131.2, 128.6, 124.7, 124.0, 120.7, 111.1, 101.5, 55.5; MS (EI)  $m/z$  336  $[\text{M}]^+$ .

#### 4.3.5. 1,7-Bis(3-methoxyphenyl)-heptane-3,5-dione (**2b**)

Yield: 42%, yellow powder;  $R_f = 0.34$  (petroleum ether/EtOAc (4:1)); mp 68–70 °C;  $^1\text{H}$  NMR 400 MHz ( $\text{CD}_3\text{Cl}$ ),  $\delta$  7.61 (d,  $J = 15.6$  Hz, 2H), 7.30 (t,  $J = 8.0$  Hz, 2H), 7.15 (d,  $J = 7.6$  Hz, 2H), 7.08 (s, 2H), 6.93 (d,  $J = 8.0$  Hz, 2H), 6.60 (d,  $J = 15.6$  Hz, 2H), 5.86 (s, 1H), 3.85 (s, 6H);  $^{13}\text{C}$  NMR 100 MHz ( $\text{CD}_3\text{Cl}$ ),  $\delta$  183.3, 160.0, 140.6, 136.5, 130.0, 124.4, 120.9, 116.0, 113.2, 101.9, 55.4; MS (EI)  $m/z$  336  $[\text{M}]^+$ .

#### 4.3.6. 1,7-Bis(4-methoxyphenyl)-heptane-3,5-dione (**2c**)

Yield: 41%;  $^1\text{H}$  NMR 300 MHz ( $\text{CD}_3\text{Cl}$ ),  $\delta$  7.59 (d,  $J = 15.9$  Hz, 2H), 7.50 (d,  $J = 8.1$  Hz, 4H), 6.53 (d,  $J = 8.7$  Hz, 4H), 6.47 (d,  $J = 15.9$  Hz, 2H), 5.78 (s, 1H), 3.85 (s, 6H);  $^{13}\text{C}$  NMR 75 MHz ( $\text{CD}_3\text{Cl}$ ),  $\delta$  183.3, 161.2, 140.1, 129.8, 127.7, 121.7, 114.3, 101.5, 55.4; MS (EI)  $m/z$  336  $[\text{M}]^+$ .

#### 4.3.7. 1,7-Bis(2-trifluoromethylphenyl)-heptane-3,5-dione (**3a**)

Yield: 45%, yellow powder;  $R_f = 0.45$  (petroleum ether/EtOAc (5:1)); mp 174–176 °C;  $^1\text{H}$  NMR 400 MHz ( $\text{CD}_3\text{Cl}$ ),  $\delta$  8.00 (dd,  $J = 15.6, 1.6$  Hz, 2H), 7.71–7.77 (m, 4H), 7.56 (t,  $J = 7.6$  Hz, 2H), 7.46 (t,  $J = 7.6$  Hz, 2H), 6.59 (d,  $J = 15.6$  Hz, 2H), 5.92 (s, 1H);  $^{13}\text{C}$  NMR 100 MHz ( $\text{CD}_3\text{Cl}$ ),  $\delta$  182.9, 136.2, 136.1, 133.9, 132.0, 129.4, 129.1, 128.8, 128.5, 128.1, 127.8, 126.3, 126.2, 125.4, 122.6, 101.6; HRMS (ESI)  $m/z$  413.0971  $[\text{M} + \text{H}]^+$ , calcd for 412.0898, error = 1.0 ppm.

#### 4.3.8. 1,7-Bis(3-trifluoromethylphenyl)-heptane-3,5-dione (**3b**)

Yield: 47%, yellow powder;  $R_f = 0.42$  (petroleum ether/EtOAc (5:1)); mp 154–156 °C;  $^1\text{H}$  NMR 400 MHz ( $\text{CD}_3\text{Cl}$ ),  $\delta$  7.81 (s, 2H), 7.67–7.74 (m, 4H), 7.63 (d,  $J = 7.6$  Hz, 2H), 7.52 (t,  $J = 8.0$  Hz, 2H), 6.68 (d,  $J = 15.6$  Hz, 2H), 5.90 (s, 1H);  $^{13}\text{C}$  NMR 100 MHz ( $\text{CD}_3\text{Cl}$ ),  $\delta$  182.9, 139.0, 135.7, 132.0, 131.7, 131.3, 131.0, 129.5, 127.9, 126.5, 125.7, 125.6, 125.2, 124.5, 124.4, 122.5, 102.4, 102.3; HRMS (ESI)  $m/z$  413.0979  $[\text{M} + \text{H}]^+$ , calcd for 412.0898, error = 1.9 ppm.

#### 4.3.9. 1,7-Bis(4-trifluoromethylphenyl)-heptane-3,5-dione (**3c**)

Yield: 51%, yellow powder;  $R_f = 0.44$  (petroleum ether/EtOAc (5:1)); mp 168–170 °C;  $^1\text{H}$  NMR 400 MHz ( $\text{CD}_3\text{Cl}$ ),  $\delta$  7.66–7.71 (m, 10H), 6.68 (d,  $J = 15.6$  Hz, 2H), 5.90 (s, 1H);  $^{13}\text{C}$  NMR 100 MHz ( $\text{CD}_3\text{Cl}$ ),  $\delta$  182.9, 139.1, 138.3, 131.8, 131.4, 128.2, 126.2, 125.9, 122.5, 102.5; HRMS (ESI)  $m/z$  413.0964  $[\text{M} + \text{H}]^+$ , calcd for 412.0898, error = 1.6 ppm.

#### 4.3.10. 1,7-Bis(phenyl)-heptane-3,5-dione (**4a**) [27]

Yield: 68%, yellow powder;  $^1\text{H}$  NMR 300 MHz ( $\text{CD}_3\text{Cl}$ ),  $\delta$  7.65 (d,  $J = 15.9$  Hz, 2H), 7.55–7.58 (m, 4H), 7.38–7.42 (m, 6H), 6.61 (d,  $J = 15.6$  Hz, 2H), 5.86 (s, 1H);  $^{13}\text{C}$  NMR 75 MHz ( $\text{CD}_3\text{Cl}$ ),  $\delta$  183.3, 140.6, 134.9, 130.1, 128.9, 128.1, 124.0, 101.8; MS (EI)  $m/z$  276  $[\text{M}]^+$ .

## 4.4. Biology method

### 4.4.1. Cell culture

Human liver hepatocellular carcinoma cells (HepG2) was purchased from the Shanghai Institute of Biochemistry and Cell Biology, Chinese Academy of Sciences and cultivated in RPMI 1640 supplemented with 2 mM glutamine, 10% (v/v) heat-inactivated fetal calf serum, 100 kU/L penicillin and 100 kU/L streptomycin at 37 °C in a humidified atmosphere with 95% air and 5%  $\text{CO}_2$ .

### 4.4.2. MTT assay

The cell viability was assessed by MTT colorimetric assay as described previously [24]. Cell viability was determined by a colorimetric assay using MTT. HepG2 cells were seeded at a density of  $3 \times 10^3$ /well in a complete growth medium in 96-well plates and incubated for 24 h. The cells were incubated with the test compounds for 48 h before the MTT assay. A fresh solution of MTT (0.5 mg/mL) was added to each single well of the 96-well plate. The plate was then incubated in a  $\text{CO}_2$  incubator for 4 h. The cells were dissolved with 100  $\mu\text{L}$  of DMSO and then analyzed in a multiwell-plate reader (Bio-Rad M680) at 570 nm.

### 4.4.3. Cell apoptosis analysis

HepG2 cells ( $5 \times 10^5$ /well) were plated in six-well plates and incubated for 24 h to allow exponential growth, then treated with test compounds for 24 h. When necessary, the cells were pretreated with GSH or NAC for 1 h before adding test compounds. The treated cells were collected and labeled with Annexin V-FITC/PI according to the manufacturer's instructions. A total of 10,000 cells per sample were collected and analyzed by FACSDiva software.

### 4.4.4. Measurement for intracellular ROS levels

Intracellular ROS levels were determined according to 2',7'-dichlorofluorescein fluorescence assay as described previously [24]. After 3 or 6 h of treatment with test compounds, HepG2 cells were incubated with 3  $\mu\text{M}$  DCFH-DA for 30 min at 37 °C in the dark. Then the cells were washed with PBS and analyzed immediately for 2',7'-

dichlorofluorescein fluorescence intensity with a FACSCanto flow cytometer with excitation and emission settings of 488 and 530 nm, respectively. When necessary, the cells were pretreated with GSH (1 h) or NAC (1 h) before adding test compounds.

#### 4.4.5. Measurement of GSH and GSSG levels

HepG2 cells at a density of  $5 \times 10^5$  per well were grown in six-well plates for 24 h, after 6 h of treatment with **1b** at the indicated concentrations, the cells were collected, resuspended in 500  $\mu$ L of ice-cold HCl (10 mM) and lysed by three cycles of freezing and thawing using liquid nitrogen and a 37 °C water bath, respectively. Twenty microliter aliquot of the lysate was used for protein determination. The remaining protein was subsequently precipitated by adding 120  $\mu$ L of ice-cold 5-sulfosalicylic acid (SSA, 6.5%, w/v) for 10 min and removed by centrifugation for 15 min (8000 g, at 4 °C). The resulting supernatant was collected and assayed for total GSH and GSSG according to the glutathione reductase-DTNB recycling assay as described previously [24].

#### 4.4.6. Measurement of lipid peroxidation

Lipid peroxidation was measured according to the protocol as described previously [24]. HepG2 cells were seeded at a density of  $5 \times 10^5$  per well in six-well plates and allowed to grow for 24 h. After 18 h treatment with **1b** (6.25, 25, 37.5 and 50  $\mu$ M) for 18 h, the cells were harvested. Then the cells were resuspended in 200  $\mu$ L of ice-cold water and lysed by three cycles of freezing and thawing using liquid nitrogen and a 37 °C water bath, respectively. Twenty microliter aliquot of the lysate was used for protein determination and 250  $\mu$ L of assay mixture containing 0.4% (w/v) thiobarbituric acid, 0.5% (w/v) SDS and 9.4% (w/v) acetic acid (pH 3.5) was added to the remaining sample. After incubation for 1 h at 95 °C, the samples were immediately cooled to room temperature and centrifuged at 3000 g for 10 min. The absorbance of resulting supernatants was read at 532 nm and the concentration of MDA in the samples was calculated against a standard curve using the MDA standard (10 mM 1,1,3,3-tetramethoxypropane in water). Lipid peroxidation was expressed as MDA equivalence (pmol MDA/mg protein).

#### 4.4.7. Analysis of mitochondrial membrane potential

Mitochondrial membrane potential was monitored by the fluorescent dye, Rhodamine 123 as described previously [24]. Briefly, HepG2 cells ( $5 \times 10^5$ /well) were plated in six-well plates and incubated for 24 h to allow exponential growth, then the cells were treated with the test compounds at the indicated concentration for 12 or 18 h. The treated cells were collected and analyzed immediately for Rhodamine 123 fluorescence intensity by flow cytometry. When necessary, the cells were pretreated with GSH (1 h) or NAC (1 h) before adding test compounds.

## Acknowledgments

This work was supported by the National 863 project of China (Grant No. 2012AA02A306).

## Appendix A. Supplementary data

Supplementary data related to this article can be found at <http://dx.doi.org/10.1016/j.ejmech.2016.02.019>.

## References

- [1] N. Hail, M. Cortes, E.N. Drake, J.E. Spallholz, *Free Radic. Biol. Med.* 45 (2008) 97–110.
- [2] N. Hail, *Apoptosis* 10 (2005) 687–705.
- [3] S.Y. Sun, N. Hail, R. Lotan, *J. Natl. Cancer Inst.* 96 (2004) 662–672.
- [4] D. Trachootham, J. Alexandre, P. Huang, *Nat. Rev. Drug Discov.* 8 (2009) 579–591.
- [5] E.H. Sarsour, M.G. Kumar, L. Chaudhuri, A.L. Kalen, P.C. Goswami, *Antioxid. Redox. Sign.* 11 (2009) 2985–3011.
- [6] G.T. Wondrak, *Antioxid. Redox. Sign.* 11 (2009) 3013–3069.
- [7] J. Antosiewicz, W. Ziolkowski, S. Kar, A.A. Powolny, S.V. Singh, *Planta Med.* 74 (2008) 1570–1579.
- [8] H. Pelicano, D. Carney, P. Huang, *Drug Resist. Update.* 7 (2004) 97–110.
- [9] V. Jamier, L.A. Ba, C. Jacob, *Chem. Eur. J.* 16 (2010) 10920–10928.
- [10] B.C. Dickinson, C.J. Chang, *Nat. Chem. Biol.* 7 (2011) 504–511.
- [11] S.C. Gupta, S. Prasad, J.H. Kim, S. Patchva, L.J. Webb, I.K. Priyadasini, B.B. Aggarwal, *Nat. Prod. Rep.* 28 (2011) 1937–1955.
- [12] P. Anand, C. Sundaram, S. Jhurani, A.B. Kunnumakkara, B.B. Aggarwal, *Cancer Lett.* 267 (2008) 133–164.
- [13] A. Goel, S. Jhurani, B.B. Aggarwal, *Mol. Nutr. Food Res.* 52 (2008) 1010–1030.
- [14] P. Anand, B. Sung, A.B. Kunnumakkara, K.N. Rajasekharan, B.B. Aggarwal, *Biochem. Pharmacol.* 82 (2011) 1901–1909.
- [15] P. Anand, A.B. Kunnumakkara, R.A. Newman, B.B. Aggarwal, *Mol. Pharm.* 4 (2007) 807–818.
- [16] G. Garcea, D.J.L. Jones, R. Singh, A.R. Dennison, P.B. Farmer, R.A. Sharma, W.P. Steward, A.J. Gescher, D.P. Berry, *Br. J. Cancer* 90 (2004) 1011–1015.
- [17] B.K. Adams, E.M. Ferstl, M.C. Davis, M. Herold, S. Kurtkaya, R.F. Camalier, M.G. Hollingshead, G. Kaur, E.A. Sausville, F.R. Rickles, J. Pl Snyder, D.C. Liotta, M. Shoji, *Bioorgan. Med. Chem.* 12 (2004) 3871–3883.
- [18] Y. Wang, J. Xiao, H. Zhou, S. Yang, X. Wu, C. Jiang, Y. Zhao, D.L. Liang, X.K. Li, G. Liang, *J. Med. Chem.* 54 (2011) 3768–3778.
- [19] T.P. Robinson, T. Ehlers, R.B. Hubbard, X.H. Bai, J.L. Arbiser, D.J. Goldsmith, J.P. Bowen, *Bioorgan. Med. Chem. Lett.* 13 (2003) 115–117.
- [20] S.M. Bayomi, H.A. El-Kashef, M.B. El-Ashmawy, M.N.A. Nasr, M.A. El-Sherbeny, N.I. Abdel-Aziz, Magda A.-A. El-Sayed, G.M. Suddek, S.M. El-Messery, M.A. Ghaly, *Eur. J. Med. Chem.* 101 (2015) 584–594.
- [21] Q.Y. Li, J. Chen, S.Y. Luo, J.L. Xu, Q.X. Huang, T.Y. Liu, *Eur. J. Med. Chem.* 93 (2015) 461–469.
- [22] N.K. Paul, M. Jha, K.S. Bhullar, H.P. Vasantha Rupasinghe, J. Balzarini, A. Jha, *Eur. J. Med. Chem.* 87 (2015) 461–470.
- [23] P.R. Baldwin, A.Z. Reeves, K.R. Powell, R.J. Napier, A.I. Swimm, A.S. Kyle Giesler, B. Bommarius, T.M. Shinnick, J.P. Snyder, D.C. Liotta, D. Kalman, *Eur. J. Med. Chem.* 92 (2015) 693–699.
- [24] F. Dai, G.Y. Liu, Y. Li, W.J. Yan, Q. Wang, J. Yang, D.L. Lu, D.J. Ding, D. Lin, B. Zhou, *Free Radic. Biol. Med.* 85 (2015) 127–137.
- [25] F.Q. Schafer, G.R. Buettner, *Free Radic. Biol. Med.* 30 (2001) 1191–1212.
- [26] Y.J. Shang, X.L. Jin, X.L. Shang, J.J. Tang, G.Y. Liu, F. Dai, Y.P. Qian, G.J. Fan, Q. Liu, B. Zhou, *Food Chem.* 119 (2010) 1435–1442.
- [27] Q.Y. Wei, W.F. Chen, B. Zhou, L. Yang, Z.L. Liu, *BBA-Gen Subj.* 1760 (2006) 70–77.